Structures, Electronic Properties, and Isomerization of the HCCCO Radical

ARTICLE *in* THE JOURNAL OF PHYSICAL CHEMISTRY · JULY 1995

Impact Factor: 2.78 · DOI: 10.1021/j100028a009

4 AUTHORS, INCLUDING:

Andrew L Cooksy
San Diego State University
63 PUBLICATIONS **1,395** CITATIONS

SEE PROFILE

Structures, Electronic Properties, and Isomerization of the HCCCO Radical

A. L. Cooksy*

Department of Chemistry, University of Mississippi, University, Mississippi 38677

F.-M. Tao and W. Klemperer

Department of Chemistry, Harvard University, Cambridge, Massachusetts 02138

P. Thaddeus

Division of Applied Sciences, Harvard University, Cambridge, Massachusetts 02138, and Harvard-Smithsonian Center for Astrophysics, Cambridge, Massachusetts 02138

Received: March 1, 1995; In Final Form: May 11, 1995[⊗]

The free radical HCCCO exhibits two distinct minima on the potential surface of the X^2A' ground electronic state, corresponding to two favorable, nonequivalent canonical structures: propynonyl (acetylenic) and propadienonyl (cumulenic). The geometries at these minima and the isomerization coordinate that couples them are characterized by *ab initio* calculations at Hartree−Fock and configuration interaction (CISD and QCISD) levels. At the QCISD/6-311G** level, the propynonyl structure has parameters r_{HC_a} = 1.067 Å, $r_{C_aC_b}$ = 1.213 Å, $r_{C_bC_c}$ = 1.435 Å, r_{C_cO} = 1.183 Å, θ_{HCC} = 176.9°, θ_{CCC} = 168.5°, and θ_{CCO} = 133.3°. Coupled cluster [CCSD and CCSD(T)] calculations of the relative energies were carried out at the QCISD optimized geometries. The propynonyl structure is consistently found to be the most stable, in qualitative agreement with recent experiments [*J. Chem. Phys.* **1994**, *101*, 178]. At the highest level of theory used, the propadienonyl structure is predicted to lie 12.5 kJ mol^{-1} higher in stabilization energy. The $^2A''$ excited Renner−Teller state is found to be linear, with adiabatic and vertical stabilization energies of 25.6 and 165 kJ mol^{-1}, respectively, relative to the X^2A' equilibrium structure. Discrepancies between the experimental geometry and predicted equilibrium geometry are tentatively ascribed to vibrational averaging on the extremely anharmonic bending potential surface. Predicted harmonic vibrational frequencies, permanent dipole moments, and Fermi contact terms are reported, with comparison to experimental results when possible.

Introduction

In certain carbon chain free radicals, relocation of an unpaired electron from one radical center to another can be accompanied by a change in the molecular orbital hybridization of the center atoms, resulting in significant bond angle and bond order changes without breaking any bonds. If two such structures correspond to local minima on the potential energy surface of the same electronic state, they may be considered distinct isomers rather than resonance structures. Recent *ab initio* calculations indicate that multiple minima may be a common characteristic of several $^2A'$ ground state free radicals.[1]

The HCCCO radical appears to be the first such candidate for which extensive experimental characterization is forthcoming. The two canonical structures for HCCCO are drawn in Figure 1: the propynonyl radical, with an acetylenic carbon chain and the unpaired electron localized at the carbon atom adjacent to the oxygen, and the propadienonyl radical, a cumulene with the unpaired electron at the carbon atom adjacent to hydrogen. The two structures both lie on the potential energy surface for the X^2A' ground state, and the minimum-energy path between them we shall call the isomerization coordinate. Motion along this path from propynonyl to propadienonyl does not alter the sequence of the atoms, but shifts the unpaired electron from the C_c atom to the C_a atom and changes the orbital hybridization of the C_c atom from sp^2 to sp and the C_a from sp to sp^2, where the carbon atoms have been labeled in the order $HC_aC_bC_cO$. In this respect, the isomerization is analogous to the conversion of propynal (HCCCHO) to propadienone (H_2CCCO) but with the shifting H bond replaced by the unpaired electron.

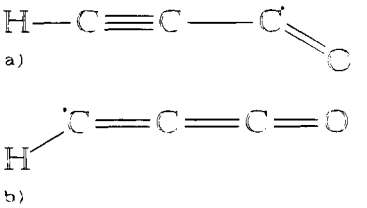

Figure 1. Two isomers of HCCCO in the X^2A' ground state: (a) propynonyl and (b) propadienonyl radical.

Experimental characterization of HCCCO was motivated by indications of its importance in combustion chemistry,[2] photochemistry,[3] and interstellar chemistry.[4] The molecule was first observed directly by rotational spectroscopy of an acetylene−carbon monoxide discharge, and its assignment was confirmed by detection of the deuterium isotopomer.[5,6] The rotational constants were consistent with the *ab initio* geometry, resembling propadienonyl, reported by Tomašić and Scuseria,[7] but subsequent measurement of the full series of monosubstituted isotopomers firmly established that the observed, presumably ground state, geometry was essentially that of propynonyl.[8] Rotational studies have remained confined to the ground vibrational state, but the ν_2 vibrational fundamental has been detected in an argon matrix by Jiang and Graham and verified by isotopic substitution.[9] These recent experimental results make it possible to assess the application of *ab initio* techniques to HCCCO. If sufficiently accurate, the calculations will assist experimental determination of a challenging potential energy surface.

In this report, we describe the *ab initio* characterization of both X^2A' configurations of HCCCO and the potential energy

[⊗] Abstract published in *Advance ACS Abstracts*, June 15, 1995.

0022-3654/95/2099-11095$09.00/0

surface along the isomerization coordinate. Properties of the lowest excited $^2A''$ electronic state and their relevance to experimental results are also discussed.

The earlier theoretical study reported three stationary points on the HCCCO potential surface.[7] That work, undertaken at Hartree−Fock self-consistent-field (SCF) and configuration interaction (CI) levels, focused on identifying the thermodynamically stable structures. The isomerization coordinate and excited electronic states were not discussed, and the molecule was not characterized in the vicinity of the experimentally determined geometry[8] because of convergence to the less stable minima. However, the geometries and harmonic vibrational frequencies of the linear and propadienyl structures were determined in their work, and those results are relevant to the present study.

Methods

For open-shell molecules such as HCCCO, a high-level theoretical method and an extended basis set are essential to give reliable results. Our preliminary calculations show, however, that the SCF contribution is predominant in determining the geometry and energetics for HCCCO. This is consistent with recent results for the chain radicals H_2CCC,[10] HCCN,[11] and HNCN.[12] As a result, an electron correlation theory based on a single reference configuration, such as configuration interaction (CI) or coupled cluster (CC) theory, is appropriate for studying these molecules. In the present study, we used the CI method including single- and double-excitation configurations from an SCF reference wave function with core electrons frozen from excitation (CISD and QCISD). All methods took advantage of efficient, analytical gradient methods available in the Gaussian 92 software package[13] for locating the minimum-energy structures. The reliability of using a single reference configuration was confirmed using a complete active space SCF wave function (CASSCF) with seven electrons and eight π-type orbitals in the active space.

An extended basis set, 6-311G**, was used throughout the present study. This basis set is Pople's energy-optimized set of triple-zeta quality in the valence shell,[14] augmented with a set of d-type polarization functions for each of the heavy atoms (C and O) and p-type polarization functions for H atom.[15] Further increase of the basis set, with additional valence-shell basis functions or polarization functions up to the 6-311G(2df,-2p) basis, has negligible effect on the results. A previous study of HNCN[12] indicated that larger basis sets and higher-order treatments of the electron correlation do not significantly improve the accuracy of the calculation, given the importance of vibrational averaging, as discussed below.

Geometry optimization was carried out using analytical gradient techniques at the SCF, CASSCF, CISD, and QCISD levels. For the X^2A' state of HCCCO, two local minimum-energy geometries, henceforth configurations I and II, were identified. Configuration I closely resembles the propynonyl canonical structure; configuration II resembles the propadienonyl structure. As expected for a surface with secondary minima, the initial geometry determines to which minimum the calculations converge. Attempts to choose initial conditions that converge to *cis*-bent structures failed, and the bond angles reported in this work are for fully *trans*-bent geometries. The transition state, a saddle point between the two minima, was determined by analytical gradients at the SCF level. The geometries along the isomerization coordinate were optimized for a number of fixed values of the CCO angle from 120° to 180° at both SCF and CISD levels, and the CISD and QCISD transition states were identified to within 5° of the CCO angle from these results.

Harmonic vibrational frequencies for the minimum and transition state geometries were obtained using analytic SCF second-derivative techniques and central finite differences of analytic CISD gradients. For configuration I only, these calculations were extended to the QCISD level. For the $^2A''$ state, a linear equilibrium geometry was found from geometry optimization at the SCF, CISD, and QCISD levels of theory. The permanent electric dipole moments and hyperfine Fermi contact terms of HCCCO were calculated using the CISD and QCISD densities. Finally, coupled cluster calculations including single, double, and triple excitations [CCSD and CCSD(T)] were carried out at the QCISD optimized geometries to check the stability of the predicted relative energies. All calculations were carried out using the Gaussian 92 package.[13]

Results and Discussion

X^2A' Configurations. Table 1 presents the optimized geometries and stabilization energies of configurations I and II for X^2A' HCCCO, and the QCISD/6-311G** geometries are drawn in Figure 2. It is clear from the table that the geometries of the two configurations are fairly well converged with respect to variation of the basis set beyond the 6-311G** level. The increase of basis set quality from 6-31G** to 6-311G** results in relatively large changes of the geometrical parameters. However, further increase of the 6-311G** basis set, by including either an additional set of valence basis functions (6-311++G**) or a second set of polarization functions [6-311G-(2d,2p) and 6-311G(2df,2p)], has smaller effects on the geometries. From the SCF to the CISD and QCISD levels, the geometries of both configurations are nearly conserved. The principal deviations are in the CCC and CCO angles in configuration I, with SCF and CISD values differing by as much as 7.5° using the 6-311G** basis. The QCISD values are intermediate between the SCF and CISD values for these parameters.

The CASSCF calculations, undertaken only with the 6-31G* basis set, yield optimized geometrical parameters within 0.02 Å and 3° of those obtained from SCF calculations with the same basis set. Multireference calculations therefore do not appear to substantially affect the geometries, and the energetics should be more accurately calculated by CI methods in any case. That the CASSCF calculations yield the only instance in which configuration II is more stable than I is therefore not taken to be significant.

Configurations I and II in Figure 2 can clearly be associated with the canonical structures of Figure 1. The geometry of configuration I is characterized by alternating CC bond lengths and a very bent CCO angle. The CC bond length next to CH, $r_{C_aC_b}$ = 1.213 Å, is typical of a triple bond ($r_{C\equiv C}$ = 1.208 Å in acetylene[16]), while the CC bond length next to CO, $r_{C_bC_c}$ = 1.435 Å, is typical of a single bond in the vicinity of a triple bond (r_{C-C} = 1.46 Å in propynal[17]). In contrast, configuration II has CC bond lengths $r_{C_aC_b}$ = 1.266 Å and $r_{C_bC_c}$ = 1.320 Å, roughly consistent with double bonds (r_{CC} = 1.29 and 1.31 Å in propadienone[18]). As expected from the canonical structures, the CH and CO bond lengths are quite similar in the two configurations.

This structural information establishes that configuration I is the propynonyl radical and configuration II the propadienonyl radical. Nevertheless, there are indications of breakdown of the local bonding model. The carbon chain is bent by 11.5° and 19.5° in configurations I and II, respectively, and in configuration II the HCC angle is 140.7°, significantly larger than the 120° angle associated with normal sp^2 hybrid orbitals.

For every SCF, CI, and CC calculation, configuration I is more stable than configuration II. The difference in stabilization

TABLE 1: Optimized Geometries and Stabilization Energies for X^2A' and $^2A''$ HCCCO[a]

method/basis	r_{HC_a}	$r_{C_aC_b}$	$r_{C_bC_c}$	r_{C_cO}	θ_{HCC}	θ_{CCC}	θ_{CCO}	E
				Configuration I				
SCF/6-31G**	1.058	1.207	1.409	1.167	176.3	165.8	137.6	−188.925 700
SCF/6-311G**	1.057	1.198	1.413	1.158	178.3	167.3	137.3	−188.970 555
SCF/6-311++G**	1.057	1.198	1.411	1.158	177.6	167.9	137.3	−188.974 804
SCF/6-311G(2d,2p)	1.055	1.192	1.415	1.157	177.5	167.4	136.5	−188.978 109
SCF/6-311G(2df,2p)	1.055	1.192	1.411	1.156	177.8	168.4	137.1	−188.986 257
CASSCF/6-31G*	1.057	1.216	1.425	1.170	174.3	164.9	135.1	−189.003 248
CISD/6-31G**	1.060	1.190	1.449	1.174	178.9	175.7	129.0	−189.398 301
CISD/6-311G**	1.061	1.190	1.447	1.165	179.1	175.0	129.9	−189.468 722
QCISD/6-311G**	1.067	1.213	1.435	1.183	176.9	168.5	133.3	−189.550 087
expt (ref 8)	1.060(18)	1.219(3)	1.387(5)	1.192(2)	168(7)	163(2)	136.5(6)	
				Configuration II				
SCF/6-31G**	1.067	1.279	1.312	1.159	140.7	156.8	165.6	−188.922 656
SCF/6-311G**	1.068	1.275	1.295	1.148	140.2	162.5	172.6	−188.968 066
SCF/6-311++G**	1.068	1.274	1.295	1.148	140.8	163.6	173.0	−188.971 391
SCF/6-311G(2d,2p)	1.066	1.272	1.302	1.147	140.1	157.7	168.9	−188.974 213
SCF/6-311G(2df,2p)	1.067	1.269	1.293	1.146	140.9	164.1	173.5	−188.985 861
CASSCF/6-31G*	1.067	1.277	1.334	1.156	137.8	152.7	164.8	−189.010 904
CISD/6-31G**	1.069	1.244	1.310	1.164	142.7	164.0	171.5	−189.388 309
CISD/6-311G**	1.072	1.241	1.305	1.153	143.5	166.7	174.6	−189.459 665
CISD/DZP (ref 7)	1.075	1.274	1.311	1.168	139.1	158.8	171.5	−189.410 39
QCISD/6-311G**	1.079	1.266	1.320	1.170	140.7	160.5	168.9	−189.543 927
				$^2A''$ Excited State				
SCF/6-311G**	1.056	1.241	1.302	1.153	180.0	180.0	180.0	−188.963 223
CISD/6-311G**	1.059	1.218	1.314	1.159	180.0	180.0	180.0	−189.457 073
CISD/DZP (ref 7)	1.063	1.242	1.317	1.177	180.0	180.0	180.0	−189.406 51
QCISD/6-311G**	1.066	1.242	1.320	1.176	180.0	180.0	180.0	−189.539 662

[a] Bond lengths are given in angstroms, angles in degrees, and energies in hartrees.

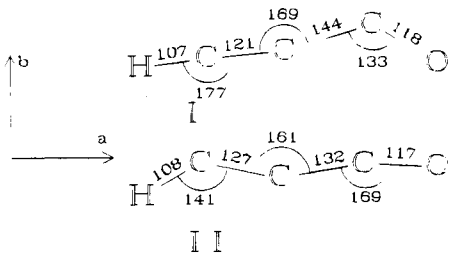

Figure 2. Predicted structures of HCCCO in the X^2A' ground state, configurations I and II in the text, based on the QCISD/6-311G** parameters in Table 1. Bond lengths are in picometers and angles in degrees.

energies between I and II is calculated at the various levels of theory to be 6.5 kJ mol^{-1} at SCF, 23.8 kJ mol^{-1} at CISD, 16.2 kJ mol^{-1} at QCISD, 16.4 kJ mol^{-1} at CCSD, and 12.5 kJ mol^{-1} at the CCSD(T) level. It is fairly certain that configuration I corresponds to the true minimum of the global potential surface for HCCCO, while configuration II corresponds to a local minimum.

The experimental geometry[8] is consistent with our results for configuration I, while the geometry of the previous *ab initio* work[7] is consistent with configuration II, as shown in Table 1. One ambiguity in the experimental analysis was the possibility that the observed spectra could also be assigned, with nearly the same quality of fit, to a second geometry which differed primarily in having a *cis*-HCCC chain. The *trans* structure was preferred based primarily on the large HC bond length, 1.10 Å, resulting from the *cis* structure fit. The present calculations support this assignment; initial geometries approximating the *cis*-HCCC structure uniformly converged to the fully *trans* structure.

The greatest deviation between experiment and the QCISD results appears to be in the bonding nature and unpaired electron distribution of the C_bC_c atom pair in configuration I. While the experimental HCC and CCO bond angles are reported with uncertainties comparable to their differences with the *ab initio* values, the CCC angle [163(2)°] and the C_bC_c bond length [1.387(5) Å] are well determined and differ markedly from the predictions (168.5° and 1.435 Å). The predicted Fermi contact terms, given in Table 2, are qualitatively correct at the QCISD level but imply a structure more closely approximating the canonical propynyl structure. The experimental Fermi contact terms are 35.8, 166.2, and 347.6 MHz for the carbon-13 nucleus at sites C_a, C_b, and C_c, respectively, stipulating that the unpaired electron is, as expected, primarily localized on the CO carbon atom. The QCISD values are 10, 213, and 378 MHz, respectively, shifting greater spin density to the C_c atom. The Fermi contact terms for configuration II follow the expected trend.

The discrepancies between experiment and predictions may be ascribed to the very anharmonic and asymmetric vibrational potential, discussed in the next section. A large C_b Fermi contact term of 363 MHz for configuration I at the CISD level was particularly puzzling, given the otherwise good agreement between configuration I and the propynonyl canonical structure. However, when the molecular geometry is constrained to the experimental parameters, the CISD Fermi contact term dropped to 228 MHz, in better agreement with experiment and illustrating the dramatic dependence of the predicted hyperfine structure on the vibrational coordinates. Test calculations on other free radicals give mixed indications of the reliability of the present hyperfine predictions. The ^{13}C Fermi contact term in the X^2A' HCO molecule was predicted to be 364 MHz at the CISD level using the 6-311G** basis, matching the experimental value of 365 MHz.[19] In HNCN,[12] however, the Fermi contact term is poorly converged even at this level of theory.

We note that the predicted *b*-axis dipole moment component of magnitude 0.70 D for configuration I is only 30% of the magnitude of the *a*-axis component, 2.39 D. Rotational transition strengths vary as the square of the transition moment, and signal-to-noise ratios for experimental measurements of the *a*-type transitions were usually in the range of 10−20. It is unlikely that the *b*-type transitions, which would deconvolute

TABLE 2: CISD and QCISD Electric Properties of X^2A' and $^2A''$ HCCCO; Principal Axes Are Oriented in the Directions Shown in Figure 2

		dipole moment (D)			Fermi contact term (MHz)				
configuration	level	μ	μ_a	μ_b	^1H	^{13}C	^{13}C	^{13}C	^{17}O
ref 8					−12	36	166	348	
I	QCISD	2.49	−2.39	0.70	1	10	213	378	−52
	CISD	2.56	−2.56	0.05	73	−86	363	335	−98
	CISD[a]	3.42	−3.35	0.69	21	−52	228	249	−114
II	QCISD	1.54	−1.17	−1.00	36	172	−43	28	−30
	CISD	1.83	−1.80	−0.36	44	155	−21	−28	−51
$^2A''$	QCISD	2.16	−2.16	0.0	−49	38	−69	5	−33
	CISD	2.39	−2.39	0.0	−38	12	−37	−34	−62

[a] CISD/6-311G** results with the geometry fixed to the experimental geometry in Table 1.

TABLE 3: Geometrical Parameters and Energies of X^2A' HCCCO along the Isomerization Coordinate at the QCISD Level[a]

θ_{CCO}	r_{HC_a}	$r_{C_aC_b}$	$r_{C_bC_c}$	r_{C_cO}	θ_{HCC}	θ_{CCC}	ΔE
120.0	1.067	1.214	1.458	1.191	177.0	174.1	10.6
133.3[b]	1.067	1.213	1.435	1.183	176.9	168.5	0.0
140.0	1.067	1.217	1.419	1.181	176.5	165.9	2.0
150.0	1.066	1.224	1.389	1.179	174.8	163.7	9.9
155.0	1.067	1.230	1.371	1.178	170.1	163.0	14.4
160.0	1.074	1.254	1.343	1.173	147.4	158.0	16.5
165.0	1.078	1.263	1.328	1.170	142.1	158.8	16.3
168.9[b]	1.079	1.266	1.320	1.170	140.7	160.5	16.2
180.0	1.080	1.266	1.309	1.170	140.9	169.2	17.7

[a] Bond lengths are given in angstroms, angles in degrees, E in hartrees, and $\Delta E = E - E(I)$ in kcal mol^{-1}. [b] Potential minimum.

some of the fitted spectroscopic constants, can be measured with the present experimental sensitivity of the discharge apparatus, although enhanced production schemes employing hydrogen abstraction may make such measurements possible.[6]

These calculations on the HCCCO radical clearly demonstrate that, for a polyatomic system with multiple stationary points, the global minimum may be missed in a limited computational search. The elementary chemical considerations discussed above should prove useful for guiding the effective and complete search in such cases.

Isomerization Surface. The transition from configuration I to II involves concerted straightening of the CCO unit while bending the HCC group. Either the CCO or HCC angle may be chosen as a coordinate for isomerization between the two configurations; at the SCF level, either choice results in the same steepest-descent pathway connecting the two configurations. In general, there may be other isomerization paths that proceed via higher energy transition states, but no evidence of these was observed in the present study. The isomerization potential of HCCCO for a number of given values for the CCO angle from $\theta_{CCO} = 120°$ to 180° is reported in Table 3 and illustrated in Figure 3. The barrier heights are reported separately in Table 4.

The isomerization potential is very flat, and the secondary minimum is extremely shallow. The QCISD barrier, relative to the global minimum, is 16.5 kJ mol^{-1} while the isomerization energy is 16.2 kJ mol^{-1}. In both the SCF and CISD calculations, the barrier is roughly 2 kJ mol^{-1} for the isomerization of II to I, dropping to the range 0.3−1.0 kJ mol^{-1} at the QCISD and CC levels. The correlation effect on the energetics of HCCCO is significant, but the SCF results are qualitatively correct.

The geometrical changes along the isomerization path are also interesting. From $\theta_{CCO} = 120°$ to 170°, the two C−C bond lengths systematically approach each other, but the HCC angle (θ_{HCC}) decreases precipitously from 170.1° to 147.4° as the CCO bond angle is changed from 155° to 160° in the QCISD

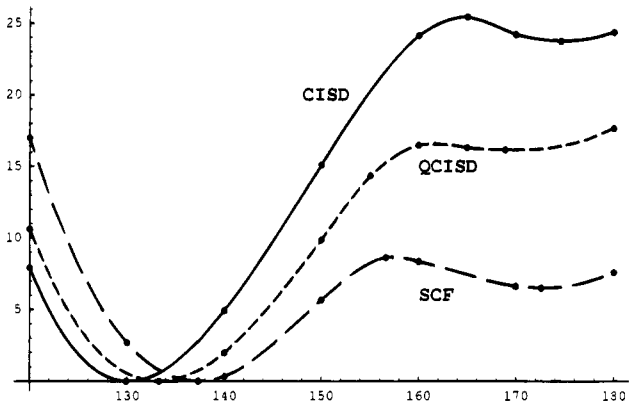

Figure 3. Potential energy curve (kJ mol^{-1}) for the isomerization coordinate (degrees θ_{CCO}) in HCCCO, determined at the SCF, CISD, and QCISD levels of theory with the 6-311G** basis, based on cubic spline plots through the discrete points indicated.

TABLE 4: Relative Energies (kJ mol^{-1}) for X^2A' and $^2A''$ HCCCO[a]

	SCF	SCF[b]	CISD	CISD[b]	QCISD	CCSD[c]	CCSD(T)[c]
$E(II) - E(I)$	6.5	3.6	23.8	14.9	16.2	16.4	12.5
$E^‡ - E(I)$	8.6	3.6	25.5	16.3	16.5	16.7	13.6
$E^‡ - E(II)$	2.1	0.04	1.7	1.4	0.3	0.3	1.0
$E(^2A'') - E(I)$	19.3		30.6		27.4	27.2	25.6
$E(^2A'')_{vert} - E(I)$	143.2		228.3		170.2	166.3	164.8

[a] $E^‡$ is the absolute energy of the transition state. [b] X^2A' relative energies corrected for the zero point vibrational energy. See text. [c] Single-point calculations carried out at the QCISD/6-311G** optimized geometries.

calculations, and analogous behavior is observed at the SCF and CISD levels (Table IS). The corresponding changes of the CH and CO bond lengths are also systematic, and the total effective bond order is approximately conserved. The CCC angle becomes quite bent (158°) at the transition state, reflecting the influence of additional canonical structures on that geometry.

In both the SCF and QCISD calculations, the linear structure and configuration II are nearly isoenergetic, and the most stable structure for $\theta_{CCO} = 180°$ is the linear structure. This is not true for the QCISD calculations, which place the linear geometry 11 kJ mol^{-1} above the energy of configuration II. For that case, there is a more stable geometry at $\theta_{CCO} = 180°$, with the parameters given in Table 3.

Harmonic Vibrational Frequencies and ZPVE Effect. Table 5 presents unscaled QCISD harmonic vibrational frequencies for configuration I. Table 6 gives the values for configurations I and II and for the transition state using the SCF and CISD potential surfaces. The lowest-frequency bending mode in HCCCO(I) is predicted to have a harmonic vibrational frequency below 250 cm^{-1}, indicative of the flat isomerization potential surface. The predicted HCC out-of-plane bending frequency drops from over 750 cm^{-1} to less than 300 cm^{-1} as

TABLE 5: Harmonic Vibrational Frequencies (cm^{-1}) and IR Intensities (km mol^{-1}) for HCCCO(I) at the QCISD Level

mode[a]	freq	IR int
CCCO asym in-plane bend	203	1
CCCO out-of-plane bend	259	2
CCCO sym in-plane bend	576	5
HCC in-plane bend	648	50
HCC out-of-plane bend	787	25
CCCO sym stretch	844	21
CO stretch	1970	195
C≡C stretch	2268	232
CH stretch	3490	40

[a] Approximate descriptions based on atomic displacements; "sym" and "asym" indicate modes corresponding approximately to modes of $D_{\infty h}$ four-atom chain that are symmetric and antisymmetric with respect to inversion.

TABLE 6: Harmonic Vibrational Frequencies (cm^{-1}) and IR Intensities (km mol^{-1}) for X^2A' HCCCO at the SCF and CISD Levels; Zero-Point Vibrational Energy, ZPVE, Is Calculated as One-Half the Sum of the Harmonic Frequencies

	SCF/6-311G**		CISD/6-311G**	
mode[a]	freq	IR int	freq	IR int
Configuration I				
CCCO asym in-plane bend	181	1	233	2
CCCO out-of-plane bend	264	4	323	4
CCCO sym in-plane bend	604	26	631	13
HCC in-plane bend	654	40	792	49
CCCO sym stretch	902	15	859	50
HCC out-of-plane bend	852	32	891	24
CO stretch	2091	298	2163	350
C≡C stretch	1959	134	2960	454
CH stretch	3590	73	3670	2
ZPVE	5548		6261	
Transition State				
CCCO asym in -plane bend	322i		219i	
CCCO out-of-plane bend	227		246	
CCCO sym in-plane bend	279		303	
HCC in-plane bend	587		551	
HCC out-of-plane bend	732		816	
CCCO sym stretch	909		987	
C≡C stretch	1683		1941	
CO stretch	2168		2449	
CH stretch	3487		3463	
ZPVE[b]	5037		5378	
Configuration II				
HCC out-of-plane bend	249	4	249	7
CCCO asym in-plane bend	237	12	260	11
CCCO sym in-plane bend	347	18	358	17
CCCO out-of-plane bend	697	59	632	132
HCC in-plane bend	774	93	734	72
CCCO sym stretch	961	1	1012	0
C_aC_b stretch	1683	24	1928	19
CO stretch	2282	848	2485	1846
CH stretch	3427	6	3413	9
ZPVE	5328		5536	

[a] Approximate descriptions based on atomic displacements; "sym" and "asym" indicate modes corresponding approximately to modes of a $D_{\infty h}$ four-atom chain that are symmetric and antisymmetric with respect to inversion. [b] For the transition state, the CCCO asym in-plane bend is neglected in calculation of the ZPVE.

the molecule deforms from I to II; roughly the reverse is seen for the CCCO out-of-plane bend. The CH and highest CC stretching frequencies also drop from configuration I to II. These frequency shifts reflect the differences in bond strength and orientation between the configurations.

The experimentally observed vibrational transition at 2308.6 cm^{-1} [9] is surprisingly high compared to the QCISD frequencies of the two strong fundamental stretching transitions for configuration I: 1970 and 2268 cm^{-1}. It is rare for the harmonic vibrational frequencies to underestimate the experimental values, and this suggests that analysis of even the higher vibrational modes may be complicated by the unusual potential surface.

The CISD harmonic frequencies are uniformly higher than the QCISD frequencies, but agreement is to within 20% for the bends and 10% for the stretches, with one exception. The CISD frequency predictions for configuration I include an extraordinarily large CC stretching frequency of 2960 cm^{-1}. The effect is also observed using the 6-31G** basis set but is not seen in the QCISD calculations nor in the CISD calculations for the other stationary points.

For features of the potential energy surface that are large compared to the fundamental vibrational frequencies, the potential in one coordinate can usually be adequately represented by the approach used to obtain Figure 3. However, with the isomerization barrier at or below about 25 kJ mol^{-1} (roughly 2000 cm^{-1}), changes in the zero-point energy of the other modes with the isomerization coordinate may profoundly influence the effective single-coordinate potential.

We therefore carry out a first-order correction to the Hartree–Fock isomerization surface reported above, according to the standard method for reducing the dimensionality of a multivariable potential surface. We assume the vibrational coordinates are all fully independent and that there is only vibrational excitation in the isomerization coordinate. The effective potential $U_{\text{eff}}^{(9)}$, on which the wave functions of the isomerization coordinate may be calculated, is given by

$$U_{\text{eff}}^{(9)} = E_0^{(1)} + E_0^{(2)} + \ldots + E_0^{(8)} + U^{(9)} \qquad (1)$$

where $U^{(i)}$ and $E_0^{(i)}$ are the potential and zero-point energy terms, respectively, for the ith vibrational mode. We estimate the zero-point energies as one-half the sum of the harmonic frequencies in modes 1–8 at each stationary point and add these to the global potential energy U at that point as determined directly from the optimization described above. The corrected barrier heights and relative energies are given in Table 4.

At the Hartree–Fock level, the result of this correction is to decrease the isomerization barrier from 8.6 to 3.6 kJ mol^{-1} and the well-depth of the secondary minimum from 2.1 to 0.04 kJ mol^{-1}. At the CISD level, the zero-point correction reduces the isomerization barrier from 25.5 to 16.3 kJ mol^{-1}, but the effect on the well depth of the secondary minimum is relatively small: a decrease from 1.7 to 1.4 kJ mol^{-1}. With the inclusion of the zero-point effect, the likelihood of configuration II being a stable structure diminishes.

These corrected values are not intended as a quantitative prediction of the true effective potential. The probable high degree of anharmonicity in the other bending modes of HCCCO argues that the model is inadequately precise, and a multidimensional analysis of the HCCCO vibrational surface to an accuracy of even 1 kJ mol^{-1} remains infeasible. Rather, we wish to emphasize the likely importance of the zero-point energy contributions to the effective isomerization potential in these problems. In particular, higher levels of theory and larger basis sets are likely to be superfluous to predictions of the molecular properties that neglect the large-amplitude, anharmonic vibrational motion.

$^2A''$ State. In addition to the complex nature of the bending potential, experimental characterization of excited vibrational states in HCCCO may be complicated by the Renner–Teller effect. The ground state of linear HCCCO has the π-electron configuration $1\pi^4 2\pi^4 3\pi$ and therefore the electronic state symmetry $^2\Pi$. Bending vibrations cause the molecule to deviate

from the linear geometry, and break the Λ symmetry of the $^2\Pi$ state. If the molecule deforms in the plane of the unpaired electron, the electronic state, now classified according to the C_s point group, is $^2A'$; if the deformation is parallel to the nodal plane of the unpaired electron, the state is $^2A''$. The energy difference between these electronic states is the Renner–Teller splitting.

The linear geometry, analyzed previously by Tomašić and Scuseria,[7] is a saddle point on the $^2A'$ ground state surface but corresponds to the minimum of the $^2A''$ surface. Optimizations at the SCF, CISD, and QCISD levels with initial geometries corresponding to configurations I and II converged to the linear structure, with the bond lengths reported in Table 1. The Fermi contact terms and dipole moments calculated at the CISD and QCISD levels are reported in Table 2. The CISD bond lengths are within 0.03 Å of those determined by Tomašić and Scuseria, and therefore we did not repeat their calculations of the CISD harmonic vibrational frequencies.

The excited $^2A''$ state has not been investigated directly by experiment, but an indirect assessment of the vertical Renner–Teller interval at the ground state geometry was made[6] using the relationship derived by Curl[20]

$$\Delta E = 4AA_{SO}/\epsilon_{aa} \quad (2)$$

where A is the largest rotational constant, A_{SO} the spin–orbit constant of the linear configuration, and ϵ_{aa} the a-axis spin-rotation constant. By this method, the vertical Renner–Teller gap ΔE in HCCCO was estimated at 2560 cm^{-1}.

For comparison, the stabilization energies of the $^2A''$ state at the equilibrium geometry of the ground $^2A'$ state was calculated. The predicted vertical Renner–Teller gap is 170 kJ mol^{-1} (14 000 cm^{-1}), excluding correction for the zero-point energy. This geometry is classically allowed to the $^2A''$ state only for vibrational levels that lie at least 12 000 cm^{-1} above the potential energy at the equilibrium $^2A''$ geometry, much higher than the zero-point energy of that electronic state. Therefore, no zero-point energy correction is made for the excited state. However, the vertical Renner–Teller gaps given above also include the $^2A'$ zero-point energy, which will not appear in the experimental value. Subtracting the contribution from zero-point energy in the ground state, roughly 6000 cm^{-1} based on the harmonic frequencies, leaves the predicted value of ΔE at 8000 cm^{-1}. Although the Curl relation is approximate, it appears that the precision of the calculations is not sufficient to adequately predict this interval.

Conclusions

Experimental advances in the characterization of hydrocarbon free radicals continue to test the *ab initio* methods on which kinetic models of combustion and interstellar chemistry have long relied. The HCCCO radical, exhibiting two distinct, nearly isoenergetic minima on the ground state potential energy surface, carries particular peril for these calculations as well as the more familiar challenges of high electron correlation and a low-lying excited electronic state. Where comparison to experiment is possible, the present calculations yield encouraging but mixed results. The geometry of the ground state is correctly predicted to have a predominantly acetylenic structure with the unpaired electron localized on the carbon atom adjacent to the oxygen. This work furthermore supports the assignment of the experimental structure to a fully *trans*-bent geometry. Finer details of the predictions—notably the HCC bond angle, the stretching frequency, and the Renner–Teller gap—do not concur with the experimental results, possibly because of vibrational effects amplified by the very flat and anharmonic bending potential.

The success of the geometrical analysis is encouraging for application of these calculations to other experiments sampling gross features of the molecule. SCF, CISD, QCISD, CCSD, and CCSD(T) methods all yield the same qualitative results, but the energy level differences are too close to the zero-point energy corrections for precise predictions of the effective isomerization barrier and relative stabilization energy. The basis set appears well converged at the 6-311G** level. The dipole moment components should be useful for determining abundances of HCCCO in interstellar clouds. The vibrational frequencies and the isomerization potential may serve as guides for future experimental studies of the potential surface.

Acknowledgment. These calculations were carried out at the Mississippi Center for Supercomputing Research and at the Cornell Theory Center, whom we thank for use of their facilities. A.L.C. thanks S.R. Davis for valuable discussions.

Supporting Information Available: One table listing the SCF and CISD geometries at selected points along the isomerization path (2 pages). Ordering information is given on any current masthead page.

References and Notes

(1) Cooksy, A. L. *J. Am. Chem. Soc.* **1995**, *117*, 1098–1104.
(2) Lander, D. R.; Unfried, K. G.; Glass, G. P.; Curl, R. F. *J. Phys. Chem.* **1990**, *94*, 7759–7763.
(3) Haas, B.-M.; Minton, T. K.; Felder, P.; Huber, J. R. *J. Phys. Chem.* **1991**, *95*, 5149–5159.
(4) Adams, N. G.; Smith, D.; Giles, D. K.; Herbst, E. *Astron. Astrophys.* **1989**, *220*, 269–271.
(5) Cooksy, A. L.; Watson, J. K. G.; Gottlieb, C. A.; Thaddeus, P. *Astrophys. J.* **1992**, *386*, L27–L30.
(6) Cooksy, A. L.; Watson, J. K. G.; Gottlieb, C. A.; Thaddeus, P. *J. Mol. Spectrosc.* **1992**, *153*, 610–626.
(7) Tomašić, Z. A.; Scuseria, G. E. *J. Phys. Chem.* **1991**, *95*, 6905–6908.
(8) Cooksy, A. L.; Watson, J. K. G.; Gottlieb, C. A.; Thaddeus, P. *J. Chem. Phys.* **1994**, *101*, 178–186.
(9) Jiang, Q.; Graham, W. R. M. *J. Chem. Phys.* **1993**, *98*, 9251–9255.
(10) Raghavachari, K.; Trucks, G. W.; Pople, J. A.; Head-Gordon, M. *Chem. Phys. Lett.* **1989**, *157*, 479–483.
(11) Seidl, E. T.; Schaefer, H. F. *J. Chem. Phys.* **1992**, *96*, 4449–4452.
(12) Tao, F.-M.; Klemperer, W.; McCarthy, M. C.; Gottlieb, C. A.; Thaddeus, P. *J. Chem. Phys.* **1994**, *100*, 3691–3694.
(13) Gaussian 92, Revision C; Frisch, M. J.; Trucks, G. W.; Head-Gordon, M.; Gill, P. M. W.; Wong, M. W.; Foresman, J. B.; Johnson, B. G.; Schlegel, H. B.; Robb, M. A.; Replogle, E. S.; Gomperts, R.; Andres, J. L.; Raghavachari, K.; Binkley, J. S.; Gonzalez, C.; Martin, R. L.; Fox, D. J.; Defrees, D. J.; Baker, J.; Stewart, J. J. P.; Pople, J. A. Gaussian, Inc., Pittsburgh, PA, 1992.
(14) Krishnan, R.; Binkley, J. S.; Seeger, R.; Pople, J. A. *J. Chem. Phys.* **1980**, *72*, 650–654.
(15) Frisch, M. J.; Pople, J. A.; Binkley, J. S. *J. Chem. Phys.* **1984**, *80*, 3265–3269.
(16) Harmony, M. D.; Laurie, V. W.; Kuczkowski, R. L.; Schwendeman, R. H.; Ramsay, D. A.; Lovas, F. J.; Lafferty, W. J.; Maki, A. G. *J. Phys. Chem. Ref. Data* **1987**, *8*, 619–721.
(17) Brand, J. C. D.; Chan, W. H.; Liu, D. S.; Callomon, J. H.; Watson, J. K. G. *J. Mol. Spectrosc.* **1974**, *50*, 304–309.
(18) Brown, R. D.; Godfrey, P. D.; Champion, R. *J. Mol. Spectrosc.* **1987**, *123*, 93–125.
(19) Holmberg, R. W. *J. Chem. Phys.* **1969**, *51*, 3255–3260.
(20) Curl, R. F. *Mol. Phys.* **1965**, *9*, 585–597.

JP9505993